APPLYING THE DFT METHOD, CONSIDER THE PROPERTIES OF Sc DOPED WITH ASiNRs

Nguyen Thanh Tung[(1)], Huynh Minh Phu[(1)]

(1) Thu Dau Mot University
Corresponding author: nttung@tdm.edu.vn

DOI: 10.37550/tdmu.EJS/2024.02.543

Article Info

Volume: 6
Issue: 02
June 2024
Received: Mar.25th, 2024
Accepted: April, 1st, 2024
Page No: 179-186

Abstract

Investigating the characteristics of the three-step sorption of Sc on armchair silicene nanoribbons is the aim of this study. Since absorbed energy is the largest of the bridge, hollow, valley, and top positions, the hollow position is selected first. The structural state of the second step has an energy of adsorption of 4.18 Å and a bond length of 2.36 Å for Si-Si. Finally, ASiNRs with a high Sc atom had their 1.25 Å surface modified. Adsorbed ASiNRs resulted in new materials with semi-metal and magnetic characteristics, suggesting potential use in spintronic and electronic devices in the future.

Keywords: adsorbed Sc, adsorption chemical, electronic devices, semi-metal, spintronic devices

1. Introduction

A lot of research has been done recently on silicene as an option for graphene in the creation of new generational devices (Lin, Ni, 2012; Houssa et al., 2010). Graphene has more properties, such as high electronic conductivity and structural simplicity, but it is incompatible with silicon-based electrical circuits. Silicene, which has more properties resembling those of graphene, has garnered a lot of interest as a means of improving the compatibility of silicon-based technologies (Shao et al., 2013; Cahangirov et al., 2009). Recently, silicene has been synthesized experimentally on Ag and Ir and displays a 2D structure with buckling in the Si-Si bond (Cahangirov et al., 2013; Meng et al., 2013; Feng et al., 2012; Chen et al., 2012; Lin et al., 2012). In addition to the compatibility benefit we already talked about, silicene is better for use in electrical devices, which makes the quantum spin hall effect more likely (Drummond et al., 2012; Ezawa, 2012). Thus, studies on the electrical properties of silicene may be used in spintronics, optoelectronics, and quantum electronics (AwSchalom et al., 2007; I. zˇutic´et al., 2004; Wolf et al., 2001). To utilize silicene's advantageous electrical properties, especially those related to the band gap in new devices, it is imperative to investigate the band-gap opening in the material. Many methods have been tried to alter the band gap, including defect generation and impurity doping (Kang et al., 2014). These methods can be applied to create a half-metallic or half-conducting gap spanning the Fermi level. Many methods were used to change the band gap by using silicene (Quhe et al., 2012; Gao et al., 2013). This may aid in the production of potentially valuable piezoelectric materials (Zhang et al., 2021). The totally encased Sc clusters are magic clusters that are stable in both heat and chemicals, according to research on chemical bonding and relative stability (Liu et al., 2018). Furthermore, the results show that adding Sc changes the electrical and optical properties of CdS clusters, as well as the HOMO-LUMO gap (Rehman et al., 2015). An investigation of the RF indicates that a change in the thickness of the Sc layer will have a substantial impact on a larger transconductance (Peng-lin Wang et al., 2021). Nevertheless, no simulated research has been done on the doping of Sc on SiNRs based on 1D monolayers. On the other hand, it is possible to make spin devices.

2. Computational methods

DFT computations were carried out using the Vienna ab-initio simulation program (VASP) (Kresse, Furthmller, Comput. Mater, 1996; Kresse, Furthmller, 1996). The PBM and GGA with a PAW pseudopotential technique were used to derive the exchange-correlation potential (Kresse, Joubert, 1999). It was applied to the Brillouin zone using a 1x1x12 GMP (Monkhorst, Pack, 1976) with a 400 eV cutoff energy. Using a 1×1×100 GMP k-point mesh and a Gaussian broadening technique with a width of 0.05 eV, the DOS was calculated. The atomic positions were modified and relaxed using the conjugate gradient approach until the maximal force applied to each atom was less than 0.01 $Å^{-1}$.

Electronic energy and functions:

$$\text{Delta } E = E_S - E_M - E_P \qquad (1)$$

The symbols E_S, E_P, and E_M denote the total energy of the system, pristine, and the Sc adatoms. Using a monolayer ASiNRs model as the foundation, a survey model with N of 6 is constructed using the pristine technique (see Figure.1), which yields results and diScussion.

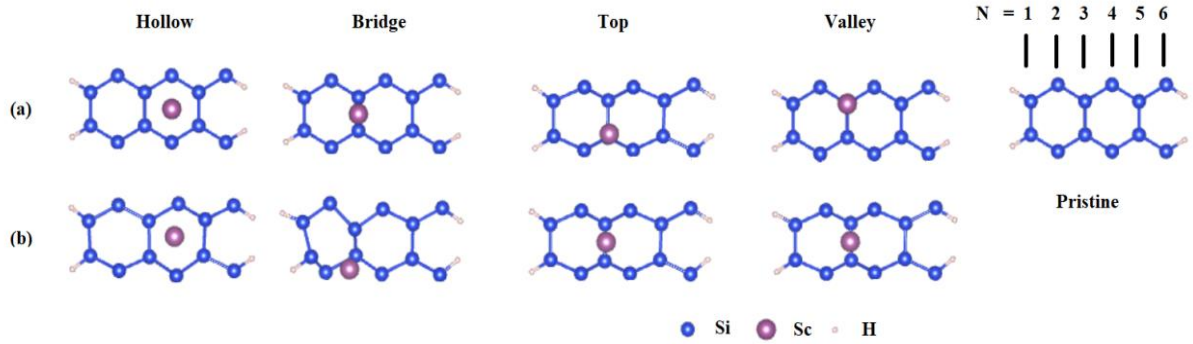

Figuge 1. Different POSCAR (a) files and CONTCAR (b) files with four positions

3. Results and discuss

3.1 Structural properties

Properties of structure 12 C and 4 H atoms are the basic building blocks of the model, and the transition metal Sc is the subject of this investigation (see Figuge.1a). The process for making a property inquiry consists of three steps. The first thing we examine is the Sc surface adhesion of pure ASiNRs in various substrates with varying Si atm link lengths. The bridge, hollow, top, and valley positions have Sc atom positioned at the height of 1.5 Å, with bond lengths from 2.20 Å to 2.35 Å. The calculations show that the hollow location has the same ASiNRs H (High) stated level, with 2.25 Å stable structural strength and an ideal energy level of -4.15 eV (see Table.1). However, despite the relatively high adsorption energy, the bridge position has fractured structures. Sc is adsorbed on ASiNR substrates in the identical bridge case, at the top and valley regions where there are fractured structures L (Low) stated, (see Figure.1 b).

TABLE 1. The energy bond ΔE at four locations of Sc doped ASiNRs

Model structures	**Si -Si bond 2.2 (A)**	**Si-Si bond 2.25 (A)**	**Si-Si bond 2.3 (A)**	**Si-Si bond 2.35 (A)**
Bridge, structure	-4.59 eV Low	-4.88 eV Low	-4.43 eV Low	-3.74 eV Low
Hollow, structure	-4.35 eV Middle	-4.15 eV High	-3.93 eV, High	-4.03 eV Middle
Valley, structure	-4.74 eV Low	-4.63 eV Low	-4.39 eV Low	-3.52 eV Middle
Top structure	-4.90 eV Low	-4.60 eV Low	-4.49 eV Low	-3.69 eV Low

The Sc atom is outside of the immaculate building with the bridge position casing. The Sc atom switched to a bridge position at the top and valley sites, indicating that structures were broken (see Figure.1b). The adsorbed Sc data obtained from ASiNRs is displayed in Table 1. In the second section of our work, we examined Sc adsorbed on ASiNRs with varying bond lengths do and hollow positions (2.20 Å to 2.30 Å and 2.35 Å). We used arithmetic to determine the optimal structure. According to Table 2, the stable bond length was 2.26 Å, the magnetic was 0.99μB, the buckling was 0.22 Å, and the adsorption energy was -4.18 eV.

TABLE 2. Result calculated with bond lengths difference of Si-Si for Sc adsorbed ASiNRs

Model structures Hollow	**Si-Si 2.2 (A)**	**Si-Si 2.22 (A)**	**Si-Si 2.24 (A)**	**Si-Si 2.26 (A)**	**Si-Si 2.28 (A)**	**Si-Si 2.30 (A)**	**Si-Si 2.35 (A)**	**Pristine**
E_P (eV)	-69.00	-69.16	-69.30	-69.41	-69.51	-69.62	-69.76	-69.56
E_M (eV)	-2.01	-1.92	-1.91	-1.81	-2.00	-1.70	-1.68	X
E_S(eV)	-75.36	-75.35	-75.38	-75.39	-75.45	-75.47	-75.47	X
Delta E (eV)	-4.35	-4.27	-4.17	-4.18	-3.94	-4.14	-4.03	X
Angle(deg)	112.04	117.29	114.37	112.45	114.02	114.02	113.40	114.46
Buckl (Å)	0.70	1.06	0.24	0.22	0.27	0.32	0.79	0.44
d_{Si-Si} (Å)	2.29	2.35	2.37	2.35	2.35	2.34	2.30	2.24
h_{Sc} (Å)	1.52	1.83	1.21	1.25	1.28	1.29	2.00	X
Mag (μ_B)	0.00	0.90	0.86	0.99	1.01	1.00	1.00	0.0
Eg(eV)	0	0	0	0.07	0	0	0	0.54
Structure states	L	M	M	H	M	M+	M	H

When Sc is adsorbed on ASiNRs, the bond length do is 2.26 Å and has the same angle Si-Si-Si as compared to pristine-structure ASiNRs; this example illustrates optimisation. Despite the fragmented structures, the bond lengths of 2.20 Å and 2.22 Å exhibit adsorption energies of -4.35 eV and -4.27 eV, respectively. But bond lengths of 2.28 Å, 2.3 Å, and 2.35 Å are also broken. Table 2 shows the outcome of the Si-Si bond length difference calculation for Sc adsorbed on ASiNRs. The height difference of Sc when adsorbed on ASiNRs is the final item we examine. The height range of the investigation was 6.1 Å to 7.9 Å. Refer to Table 3 for the results. At 6.7 Å, bond energy -4.09 eV, and magne 1.0μB, it is more stable and has a greater value than at the other heights. The outcome of deducting pristine from the height difference ho of the Sc adatom is shown in Table 3.

TABLE 3. Result calculated with the heights h_0 difference of Sc adatom on subtracting pristine

ho (Å)	7.9	7.7	7.5	7.3	7.1	6.9	6.7	6.5	6.3	6.1
E_P(eV)	-69.62	-69.62	-69.62	-69.62	-69.62	-69.62	-69.62	-69.62	-69.62	-69.62
E_M (eV)	-1.98	-1.89	-1.89	-1.88	-1.91	-2.00	-1.78	-1.86	-1.90	-2.00
E_S(eV)	-75.43	-75.48	-75.48	-75.48	-75.45	-75.50	-75.48	-75.50	-75.49	-75.50
Delta E (eV)	-3.82	-3.97	-3.97	-3.98	-3.92	-3.88	-4.09	-4.01	-3.97	-3.88
Mag (μ_B)	1.0029	1.0004	1.0022	1.0117	1.0113	1.0054	1.0040	1.0022	1.0020	1.0095

3.2 Electrical properties

The electronic band structure is a crucial quantity to consider when analysing electronic features. The orbitals projected in the 1D electronic band structure of ASiNRs are displayed in Figure 2. A short dash in red, a brown line for Si-4s, an olive line for Si-3p, and an orange line for Si-3d represent each electronic state. The Fermi level is at zero energy. The energy zone of the Brillouin zone, which extends from G to K and from -8 eV to 3 eV, has been chosen for this investigation. The Si-4s, Si-3p, and Si-3d orbital levels are related to the band structure of virgin ASiNRs. ASiNRs are semiconductors with a band gap pristine of 0.54 eV (see Figure.2).

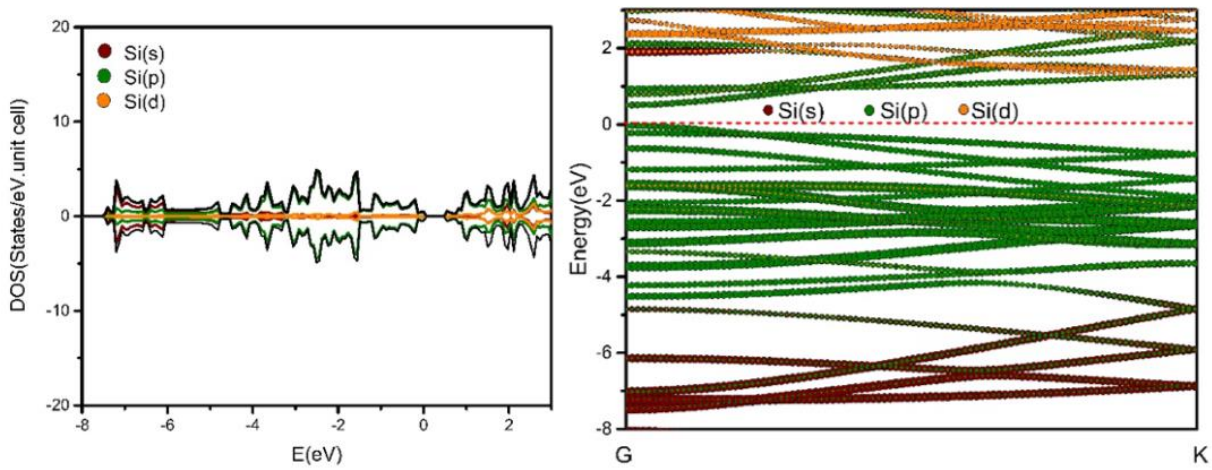

Figure 2. Shows the band structure and DOS structure of ASiNRs.

The electrons on the brown line represent the Si-4s states of silicon atoms, and the electrons on the olive line represent the Si-3p states. While Si-3p states are mostly found at the top and bottom of the conduction band (around the Fermi level), Si-4s is concentrated at the bottom of the valence band. Additionally, the orange line displays the concentration of Si-3d states at the top of the conduction band. Almost all of the high Si-3p state peaks in the pristine configuration correlate with energy levels of -3.66 eV, -3.05 eV, -2.49 eV, -1.56 eV, 1.01 eV, and 2.16 eV. In the pristine configuration, the highest peak of Si-4s has an energy level of -7.20 eV, whereas the highest peak of the Si-3d state is linked to an energy level of 2.60 eV. Examine Figure 3's DOS state and Figure 4's band structures for the bridge (B) configuration. The highest Si-3p state has a power peak of -1.29 eV. In comparison to the pristine arrangement, it travels 1.19 eV in a positive direction. At an energy level of -7.39 eV, the apex of the highest Si-4s state in the bridge arrangement might be found. In comparison to the pristine arrangement, its displacement is 0.20 eV in the negative direction, while the Si-3d state's peak is at its highest at 2.30 eV, 0.3 eV in the negative direction. Sc-3d of the bridge configuration has power levels of 0.87 eV and 0.59 eV, making it the highest peak produced by Sc adsorption on ASiNRs. The highest Sc-4s has an energy level of -0.84 eV at the status peak. Also, the band configurations seen in Fig. have a large number of Si-3p state vertices. The situation with hollow configuration (H) is shown in Figure. 3 together with the DOS status. The energy levels -1.13 eV, -0.48 eV, 0.83 eV, 1.34 eV, and 1.86 eV are comparable to these. It moves away from the pristine configuration and occupies states close to the fermium level, which is crucial for the transformation of semiconductor materials into metallic ones highest Si-4s state, -7.51 eV in energy, in the bridge structure. In comparison to the pristine configuration, it progressed by 0.10 eV in the negative direction, peaking at 1.77 eV in the negative direction and 0.83 eV for the Si-3d state. Sc gives rise to a rather broad state zone with two peaks and a width ranging from 0.71 eV to 1.19 eV when adsorbed on ASiNRs. The hollow structure has the highest Sc-3d, with energy levels of 0.96 eV and 0.76 eV, respectively. The Sc-4s state for this structure is weak, with a relatively tiny size and an energy level of 1.09 eV. However, in Figure 3's DOS state and Figure 4's band structures, numerous vertices of the Si-3p state are seen in the valley (V) configuration scenario.

These translate into 0.05 eV, -1.68 eV, -1.47 eV, and -2.36 eV of energy levels, in that order. By residing in a condition near the fermium level and shifting slightly to the positive side relative to its initial shape, this material aids in the transformation of semiconductors into metallic ones. At an energy level of -7.51 eV, the highest Si-4s state in the bridge design peaks. Its hollow form remains unaltered. When compared to the pristine setup, the Si-3d state in the top arrangement is quite weak. Two peaks, Sc-3d, are formed when Sc is adsorbed on ASiNRs; these peaks correspond to energy levels of 1.37 eV and 0.81 eV.

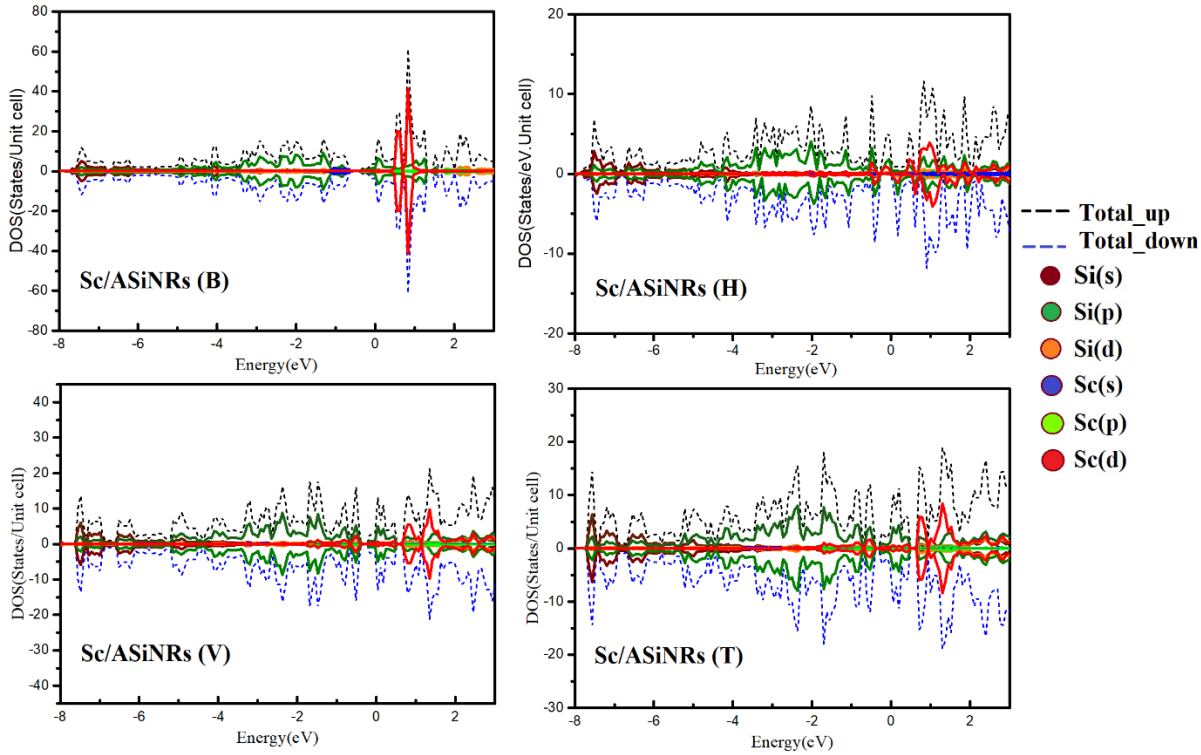

Figure 3. The DOS of the Sc/ASiNRs at the top (T), hollow (H), valley (V), and bridge (B).

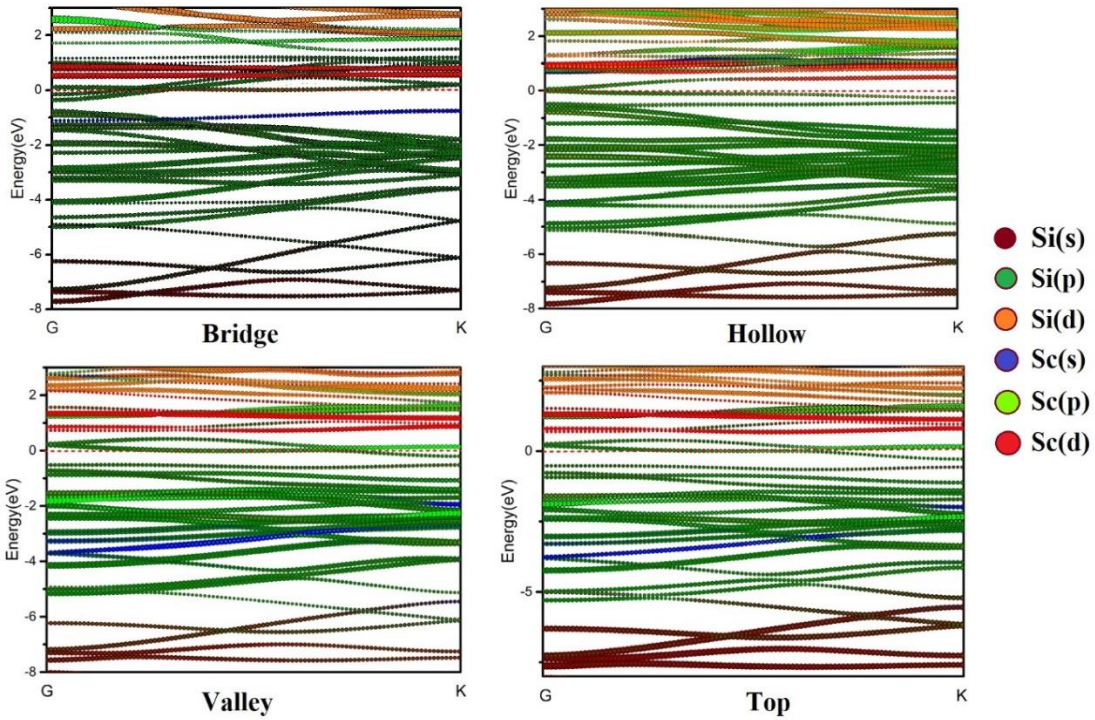

Figure 4. The Band structures of Sc adsorbed ASiNRs

The Sc-4s and Sc-3p states have no peaks and are weak in this configuration. Since the energy bands in these structures extend from the conduction band to the valence band, below the Fermi level, there is no band gap in the configuration valley. They are, hence, semi-metallic.

Lastly, we examine Figure 4's band structures and Figure 3's representation of the DOS state. The top (T) arrangement has a large number of Si-3p state vertices, as seen in Figure 4. They are in the following order of correspondence: -2.79 eV, -2.38 eV, -1.72 eV, -0.83 eV, -0.53 eV, 0.21 eV, 1.49 eV, and 2.41 eV. In comparison to the original configuration, most of these levels move in a positive

direction by about 0.8 eV. They then occupy fermi-level states that help make the material semi-metallic. at an energy level of -7.56 eV, the top structure's peak Si-4s state. It moves in the opposite direction, 0.36 eV away from the perfect arrangement. The top form's Si-3d state peaks at 2.38 eV, 0.22 eV less than the pristine configuration. Sc produces two peaks, Sc-3d, during adsorption on ASiNRs, which correspond to energy levels of 1.22 eV and 0.78 eV. Both the Sc-4s and Sc-3p states are weak in this setup.

The formula for calculating the charge displacement is deScribed as follows:

$$\Delta\sigma = \sigma_S - \sigma_M - \sigma_P \qquad (2)$$

Where σ_S is the charge density of system, σ_M is the charge density of Sc metal, and σ_P is the charge density of pristine. Combining the band and dos configurations with Figure.5 leads us to the conclusion that, of the remaining cases, the hollow configuration is the best of the structural representation of ASiNRs following Sc adsorption. Based on the charge density calculations for various configurations, as illustrated in Figure 4, we diScovered that in the pristine ASiNRs basic configuration, the initial charge density is mainly localised in the π bond between two adjacent Si-Si atoms. Sc-atom adsorption with ASiNRs alters the charge distribution of each bridge, hollow, valley, or top structure. Imagine a Scenario in which the starting arrangement is flawless, with 12 Si atoms and 4 H atoms. The primary targets of the charges are the Si-3p orbitals, which are 17.77 e/Å^3, and the Si-3s orbitals, which are 13.59 e/Å^3. A small fraction of the Si-3d orbitals is 1.39 e/Å^3. To find the charge displacement, use this formula: if the three configurations shown by the bridge configuration don't give the best results in terms of structural stability when compared to the hollow optimal form, then the Sc atom has electron densities of 0.505 e/Å^3, 0.001 e/Å^3, and 0.921 e/Å^3 for the bridge, valley, and top. Si-3s, Si-3p, and Si-3d have charge densities of 13.85 e/Å^3, 17.84 e/Å^3, and 1.56 e/Å^3, respectively, when adsorbed with ASiNRs.

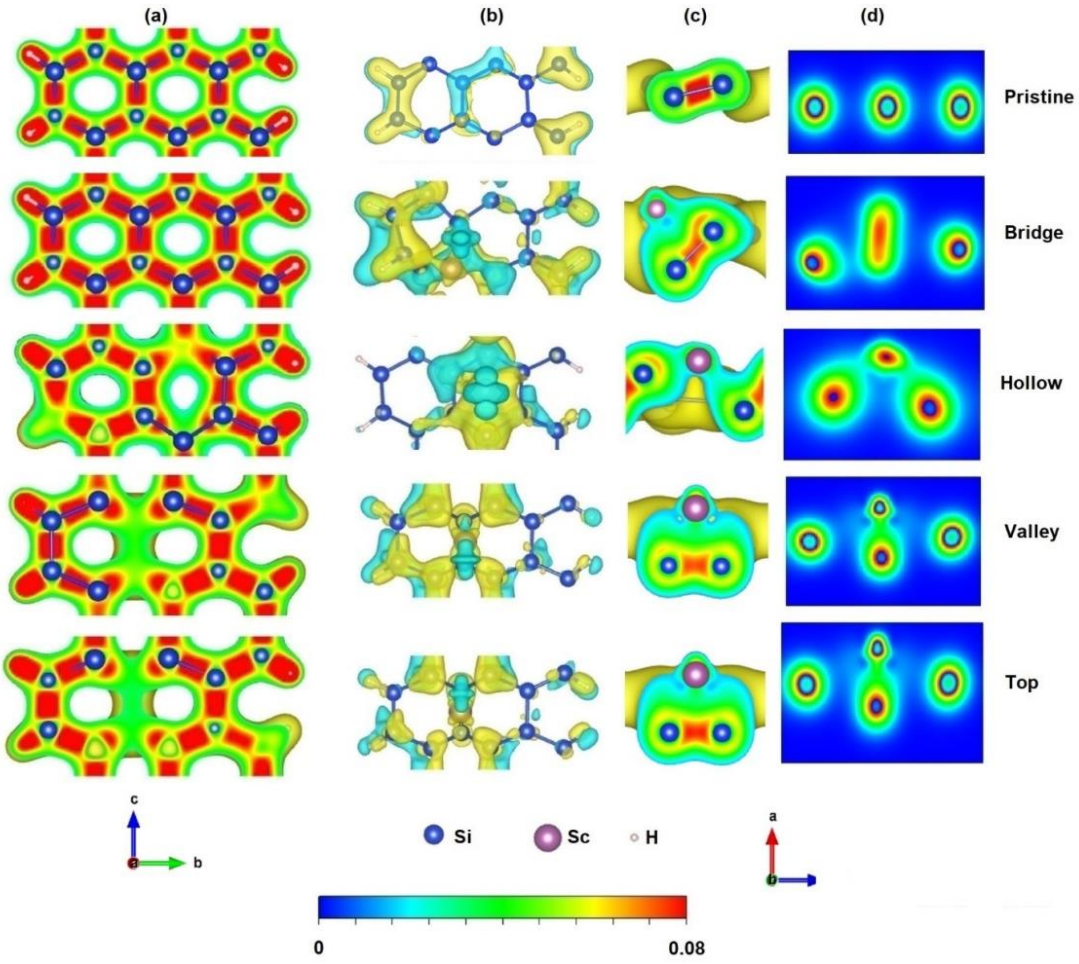

Figure 5. The charge distribution images of different configurations

This is consistent with the bands and DOS structure analysis shown in Figures 2 and 3. It also shows an increase in charge concentration as a result of a charge shift from the orbitals of Sc-4s to Si-3s. This orbital gains a significant amount of electrons through a reverse shift from the Si-3d to the Sc-3d orbital. The charge density is also more variable when the hollow form exhibits the optimum structural stability during Sc adsorption onto ASiNRs. Sc-4s has a density of 0.514 e/Å^3, Sc-3p is 0.001 e/Å^3, and Sc-3d is 0.909 e/Å^3 with the original Sc atom. Si-3s's moving charge after adsorption is 13.86 e/Å^3, while Sc-3d's and Si-3p's charge densities are 2.79 e/Å^3 and 17.73 e/Å^3, respectively. There is an obvious substantial charge transfer from the orbitals outside the Si atom to Sc in the band and DOS energy band structures that have already been examined. As a result, a powerful Sc-3d state is produced. This modification sets the hollow configuration apart from the other variants.

4. Conclusion

Since there have been no prior research investigations or publications on Sc adsorption on ASiNRs, this is a fresh attempt aimed at understanding this process. We find that the hollow configuration is the most optimal among the surveyed and calculated configurations after three steps of survey and analysis on four selected configurations. The findings show that Sc andiandi doping dramatically modifies ASiNRs' band gap. Originally a semiconductor, the unique material exhibits semi-metallic behaviour and an exceptionally narrow band gap when doped in three different configurations: valley, top, and bridge positions, especially in hollow structures. However, the hollow design also yields the best magnetic performance under other circumstances. Spin devices and next-generation electronics might benefit from the use of this novel material.

This work was conducted at Thu Dau Mot University's high-performance computing cluster (HPCC) in Binh Duong Province, Vietnam.

References

B. Feng, Z. Ding, S. Meng, Y. Yao, X. He, P. Cheng, L. Chen, K. Wu (2012). *Evidence of Silicene in Honeycomb Structures of Silicon on Ag(111)*. Nano Lett., 12, 3507-3511. https://doi.org/10.25073/2588-1124/vnumap.4461

B. Kang, H. Liu, J. Y. Lee (2014). Oxygen adsorption on single layer graphyne: a DFT study. *Phys. Chem. Chem. Phys*, 16, 974-980. https://doi.org/10.1039/C3CP53237B

C.L. Lin, R. Arafune, K. Kawahara, N. Tsukahara, E. Minamitani, Y. Kim, N. Takagi, M. Kawai (2012). *Structure of Silicene Grown on Ag(111). Appl. Phys. Express*, 5, 045802, 10.1143/APEX.5.045802, https://doi.org/10.1063/1.4894871

D. D. AwSchalom, M. E. Flatt (2007). Challenges for semiconductor spintronics. *Nat. Phys*, 3, 153-159. https://doi.org/10.1038/nphys551

G. Kresse, D. Joubert (1999). From ultrasoft pseudopotentials to the projector augmented-wave method. *Phys. Rev. B*, 59, 1758**.** https://doi.org/10.1103/PhysRevB.59.1758

G. Kresse, J. Furthmller (1996). Comput. Mater. Efficiency of ab-initio total energy calculations for metals and semiconductors using a plane-wave basis set. *Sci*, 6, 15-50, https://doi.org/10.1016/0927-0256(96)00008-0.

G. Kresse, J. Furthmller (1996). Efficient iterative Schemes for ab initio total-energy calculations using a plane-wave basis set. *Phys. Rev. B*, 54, 11169. https://doi.org/10.1103/PhysRevB.54.11169.

H. J. Monkhorst, J. D. Pack (1976). Special points for Brillouin-zone integrations. *Phys. Rev. B*, 13, 5188-5192. https://doi.org/10.1103/PhysRevB.13.5188.

I. zˇutic´, J. Fabian, S. D. Sarma (2004). Spintronics: Fundamentals and applications. *Rev. Mod. Phys*, 76, 323. https://doi.org/10.1103/RevModPhys.76.323

J. Gao, J. Zhang, H. Liu, Q. Zhang, J. Zhao (2013). Structures, mobilities, electronic and magnetic properties of point defects in silicene. *NanoScale*, 5, 9785-9792, https://doi.org/10.1039/C3NR02826G

L. Chen, C.-C. Liu, B. Feng, X. He, P. Cheng, Z. Ding, S. Meng, Y. Yao, K. Wu (2012). *Evidence for Dirac Fermions in a Honeycomb Lattice Based on Silicon*. *Phys. Rev. Lett*, 109, 056804. https://doi.org/10.1103/PhysRevLett.109.056804

L. Meng, Y. Wang, L. Zhang, S. Du, R. Wu, L. Li, Y. Zhang, G. Li, H. Zhou, W. A. Hofer, H.-J. Gao (2013). *Buckled Silicene Formation on Ir(111). Nano Lett*, 13, 685-690, https://doi.org/10.1021/nl304347w

M. Ezawa (2012). Valley-Polarized Metals and Quantum Anomalous Hall Effect in Silicene. *Phys. Rev. Lett*, 109, 055502. https://doi.org/10.1103/PhysRevLett.109.055502

M. Houssa, G. Pourtois, V. Afanasev, A. Stesmans (2010). Free-standing silicene obtained by cooling from 2D liquid Si: structure and thermodynamic properties. *Appl. Phys. Lett*, 97, 11210-112106. http://dx.doi.org/10.1063/1.3489937.

N. Drummond, V. Zolyomi, V. Fal'Ko. (2012). Electrically tunable band gap in silicene. *Phys. Rev. B*, 85, 075423. https://doi.org/10.1103/PhysRevB.85.075423

Peng-lin Wang, Hui-qing Sun, Xiao Ding, Zhi-hui Huang, Yuan Li, Fan Xia, Xiao-yu Xia, Miao Zhang, Jian-cheng Ma, Xiu-yang Tan, Liang Xu, Zhi-you Guo (2021). Analysis of RF performance of novel Sc-doped GaN high electron-mobility transistors with air-bridge structure. *Results in Phys*, 105000. https://doi.org/10.1016/j.rinp.2021.105000

Q.Zhang, M.Chen, H.Liu, X.Zhao, X. Qin, F.Wang, Y.Tang, K. H.Yeoh, K.H.Chew, X.Sun (2021). Coexistence of ferroelectricity and ferromagnetism in Ni-doped $Al_{0.7}Sc_{0.3}N$ thin films. *Materials*, *14*(21), 6437. https://doi.org/10.1063/5.0096760

R. Quhe, R. Fei, Q. Liu, J. Zheng, H. Li, C. Xu, Z. Ni, Y. Wang, D. Yu, Z. Gao, J. Lu (2012). Tunable and sizable band gap in silicene by surface adsorption. *Sci. Rep*, 2, 853, https://doi.org/10.1038/srep00853

S. Cahangirov, M. Audiffred, P. Tang, A. Iacomino, W. Duan, G. Merino, A. Rubio (2013). Electronic structure of silicene on Ag(111): Strong hybridization effects. *Phys. Rev. B*, 88, 035432. https://doi.org/10.1103/PhysRevB.88.035432

S. Cahangirov, M. Topsakal, E. Aktrk, H. S¸ahin, S. Ciraci (2009). *Phys. Rev. Lett*, 102, 236804. https://doi.org/10.1103/PhysRevLett.102.236804

S. Wolf, D. AwSchalom, R. Buhrman, J. Daughton, S. Von Molnar, M. Roukes, A. Y. Chtchelkanova, D. Treger (2001). Spintronics: a spin-based electronics vision for the future. *Science*, 294, 1488-1495. https://doi.org/10.1126/Science.1065389

S.U. Rehman, A. Majid, N. Hassan, A. Shakoor, G. Murtaza, S.D. Khan (2015). Reversible hydrogen storage capacity of Sc and Y functionalized [1,1]paracyclophane: Insights from density functional study. *Materials Science Poland*, *33*(4), 782-791. https://arxiv.org/ftp/arxiv/papers/2202/2202.13362.pdf

X. Lin, J. Ni (2012). Much stronger binding of metal adatoms to silicene than to graphene: A first-principles study. *Phys. Rev. B*, 86, 075440. https://doi.org/10.1103/PhysRevB.86.075440

Y.Liu, J.Yang, L.Cheng (2018). Structural Stability and Evolution of Scum-Doped Silicon Clusters: Evolution of Linked to Encapsulated Structures and Its Influence on the Prediction of Electron Affinities for $ScSi_n$ (n = 4–16) Clusters. *Inorg. Chem*, 57, 20, 12934-12940. https://doi.org/10.1021/acs.inorgchem.8b02159

Z.-G. Shao, X.-S. Ye, L. Yang, C.-L. Wang (2013). First-principles calculation of intrinsic carrier mobility of silicene. *J. Appl. Phys*, 114, 093712. https://doi.org/10.1063/1.4820526.